Electronic Supplementary Material (ESI) for Journal of Materials Chemistry A.

Supporting Information

A fluorene based covalent triazine framework with high CO_2 and H_2 capture and torage capacities

Stephan Hug,[abc] Maria B. Mesch,[d] Hyunchul Oh,[e] Nadine Popp,[d] Michael Hirscher,[e] Jürgen Senker[d] and Bettina V. Lotsch*[abc]

[a] Department of Chemistry, Ludwig-Maximilians-Universität München, Butenandtstr. 5-13, 81377 Munich, Germany

[b] Max Planck Institute for Solid State Research, Heisenbergstr. 1, 70569 Stuttgart, Germany

[c] Nanosystems Initiative Munich (NIM) and Center of Nanoscience, Schellingstr. 4, 80799 Munich, Germany

[d] Inorganic Chemistry III, Universität Bayreuth, Universitätsstr. 30, 95447 Bayreuth, Germany

[e] Max Planck Institute for Intelligent Systems, Heisenbergstr. 3, 70569 Stuttgart, Germany

* Corresponding Author: E-mail: bettina.lotsch@cup.uni-muenchen.de

INDEX

1. Temperature Programs

Table S1. Temperature programs used for the *fl*-CTF synthesis.

Program	Sample	Heating rate [°C h^{-1}]	T [°C]	Holding time *t* [h]	Cooling rate[a] [°C h^{-1}]
1	*fl*-CTF300	60	300	96	10
2	*fl*-CTF350	60	350	96	10
3	*fl*-CTF400	60	400	48	10
4	*fl*-CTF500	60	500	48	10
5	*fl*-CTF600	60	600	48	10

[a]At 240 °C the oven was turned off.

2. Elemental Analysis

Table S2. Elemental Analysis of *fl*-CTFs. All values are displayed in wt%.

Sample	N	C	H
calc. *fl*-CTF	12.95	83.32	3.73
fl-CTF300	9.52	80.69	3.40
fl-CTF350	7.71	81.64	3.11
fl-CTF400	6.33	84.95	2.77
fl-CTF500	6.77	84.36	2.71
fl-CTF600	5.43	82.61	1.43

3. Powder X-Ray Diffraction

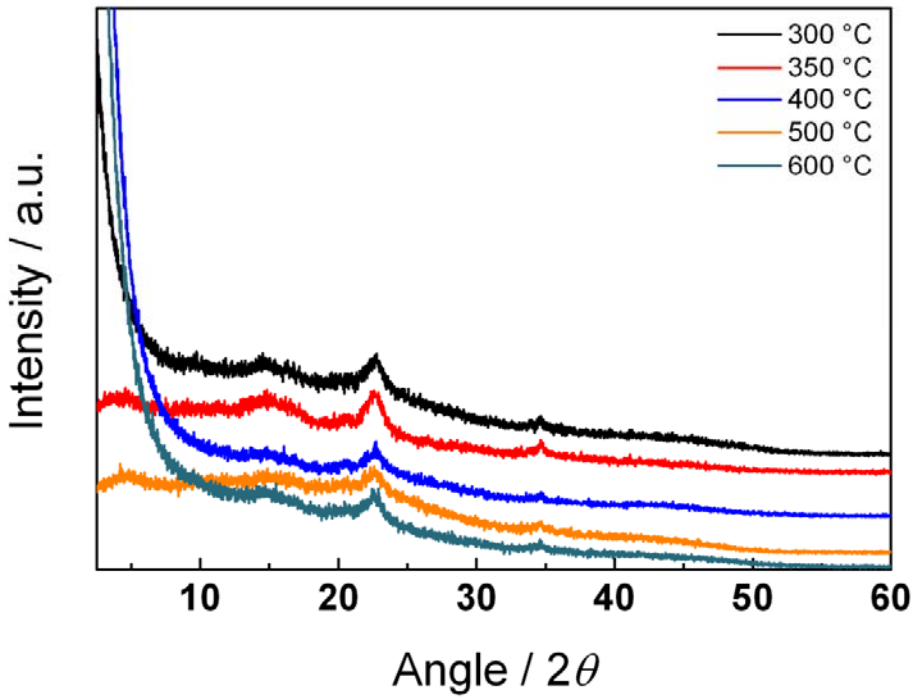

Figure S1. Powder X-Ray diffraction measurements of the samples *fl*-CTF300, *fl*-CTF350, *fl*-CTF400, *fl*-CTF500 and *fl*-CTF600.

4. Solid-State NMR Spectra

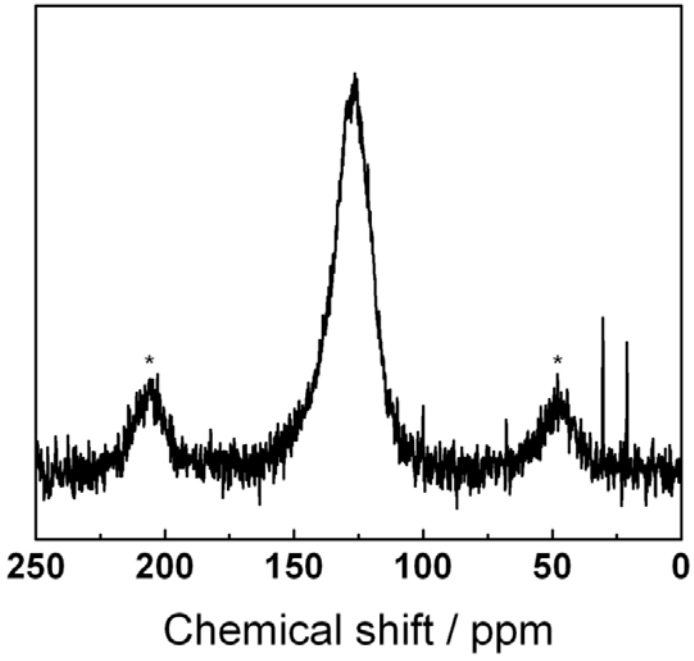

Figure S2. ^{13}C MAS ssNMR spectrum of *fl*-CTF500.

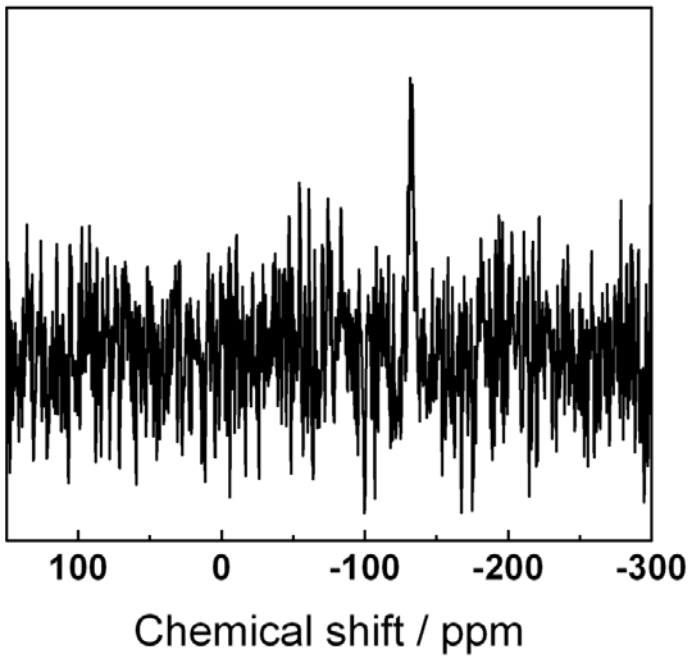

Figure S3. ^{15}N MAS ssNMR spectrum of tris(9*H*-fluoren-2-yl)-1,3,5-triazine.

c. CPPI Analysis

As the signal at 50 ppm could not be assigned to the reactant nor the product, a cross polarization with polarization inversion (CPPI) measurement[1,2] was carried out to get information about the number of covalently bonded protons. Starting from maximum magnetization it decays and becomes negative with increasing inversion time. This decay has a characteristic form according to the number of bonded protons and was fitted using the following equation[3]

$$M(\tau_i) = M^0 \left[\frac{2}{n+1} \exp\left(-\frac{\tau_i}{T_D}\right) + \frac{2n}{n+1} \exp\left(-\frac{3\tau_i}{2T_D}\right) \exp\left(-\frac{\tau_i^2}{T_C^2}\right) - 1 \right] \quad (1)$$

T_C = decay related to dipolar coupling to nearby protons
T_D = decay caused by isotropic spin-diffusion
n = number of directly bonded protons
τ_i = inversion time

The spectra of *fl*-CTF300 with increasing inversion times are displayed in Figure S4.

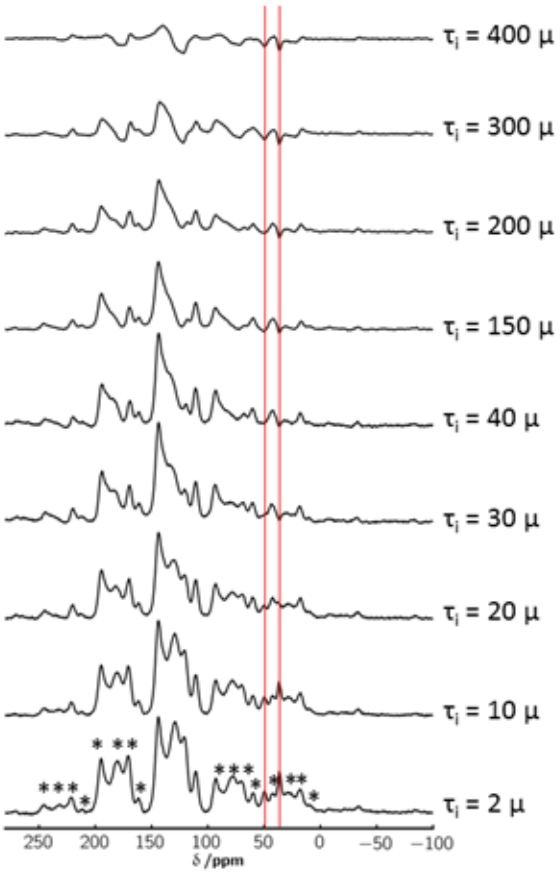

Figure S4. ^{13}C CPPI MAS ssNMR spectra of *fl*-CTF300 for different inversion times. Sidebands are marked with asterisks. Relevant signals for the CPPI experiment are indicated using red lines.

The curves extracted from the CPPI measurements are presented in Figure S5 and the relevant fitting parameters are depicted in Table S3. For the signal at 50 ppm *n* is very close to 1 and, therefore, the signal can be assigned to a CH group. For the second signal *n* is 2.45, which strongly supports the assignment to a CH_2 group. The deviation of 0.45 regarding the optimal value results from difficulties in the integration due to overlapping spinning sidebands.

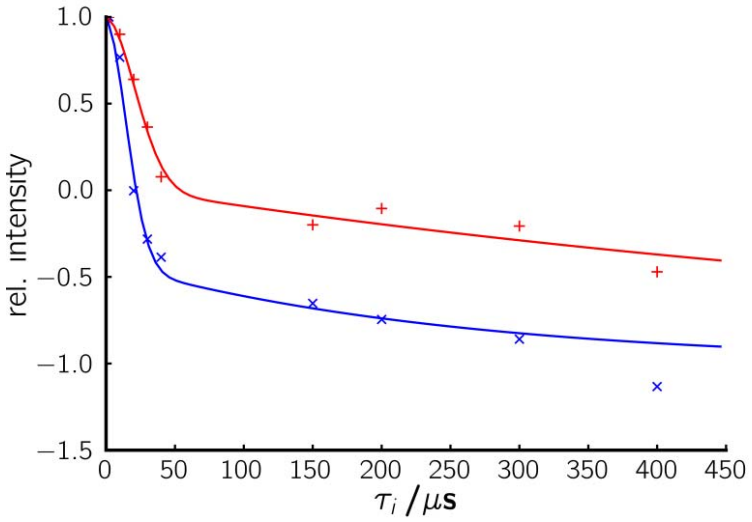

Figure S5. Normalized signal intensities plotted against the inversion time for the signal at 36.9 ppm (blue) and the signal at 50 ppm (red) of the ^{13}C MAS ssNMR CPPI spectra of *fl*-CTF300.

Table S3. Fitting parameters for the CPPI curves.

Shift / ppm	n	T_C	T_D
36.9	2.45	250.00	22.13
50	0.95	816.02	30.56

5. Argon Physisorption Measurements

Table S4. Specific Surface Areas and Pore Volumes of *fl*-CTFs.

Sample	Surface Area [$m^2\ g^{-1}$]			Pore Volume [$cm^3\ g^{-1}$]					
	BET_{Ar}	DFT_{Ar}[a]	DFT_{CO_2}[b]	$V_{Ar,mic}$[c]	$V_{Ar,mic,DFT}$[d]	$V_{Ar,tot}$[e]	$V_{Ar,tot,DFT}$[f]	$V_{CO_2,tot,DFT}$[g]	$V_{Ar,mic,DFT}/V_{Ar,tot,DFT}$
fl-CTF300	15	-	297	-	-	-	-	0.09	-
fl-CTF350	1235	1385	1020	0.48	0.57	0.69	0.67	0.33	0.85
fl-CTF400	2862	2084	1211	1.04	1.13	1.49	1.45	0.49	0.78
fl-CTF500	2322	1643	793	0.76	0.77	1.33	1.29	0.28	0.60
fl-CTF600	2113	1608	844	0.71	0.70	1.19	1.16	0.30	0.60

[a]Ar QSDFT slit pore model on carbon at 87 K. [b]CO_2 NLDFT model on carbon at 273 K. [c]Calculated pore volume at $p\ p_0^{-1} = 0.17$. [d]Pore volume for pores smaller than 2 nm calculated from the Ar QSDFT model. [e]Calculated total pore volume at $p\ p_0^{-1} = 0.95$. [f]Total pore volume from the Ar QSDFT model. [g]Total pore volume from the CO_2 NLDFT model.

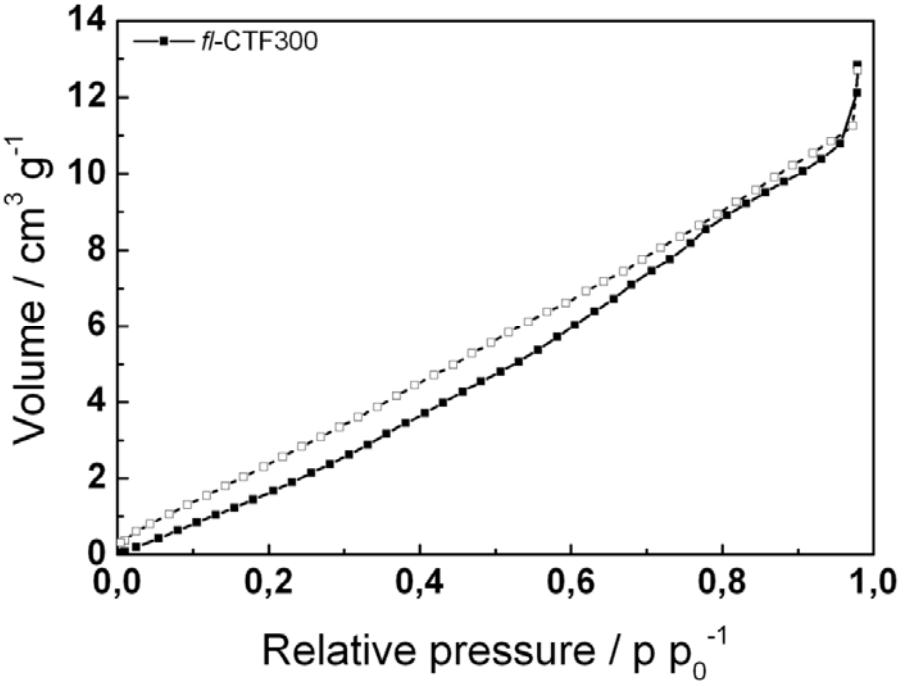

Figure S6. Argon adsorption (filled symbols) and desorption (open symbols) isotherm of *fl*-CTF300.

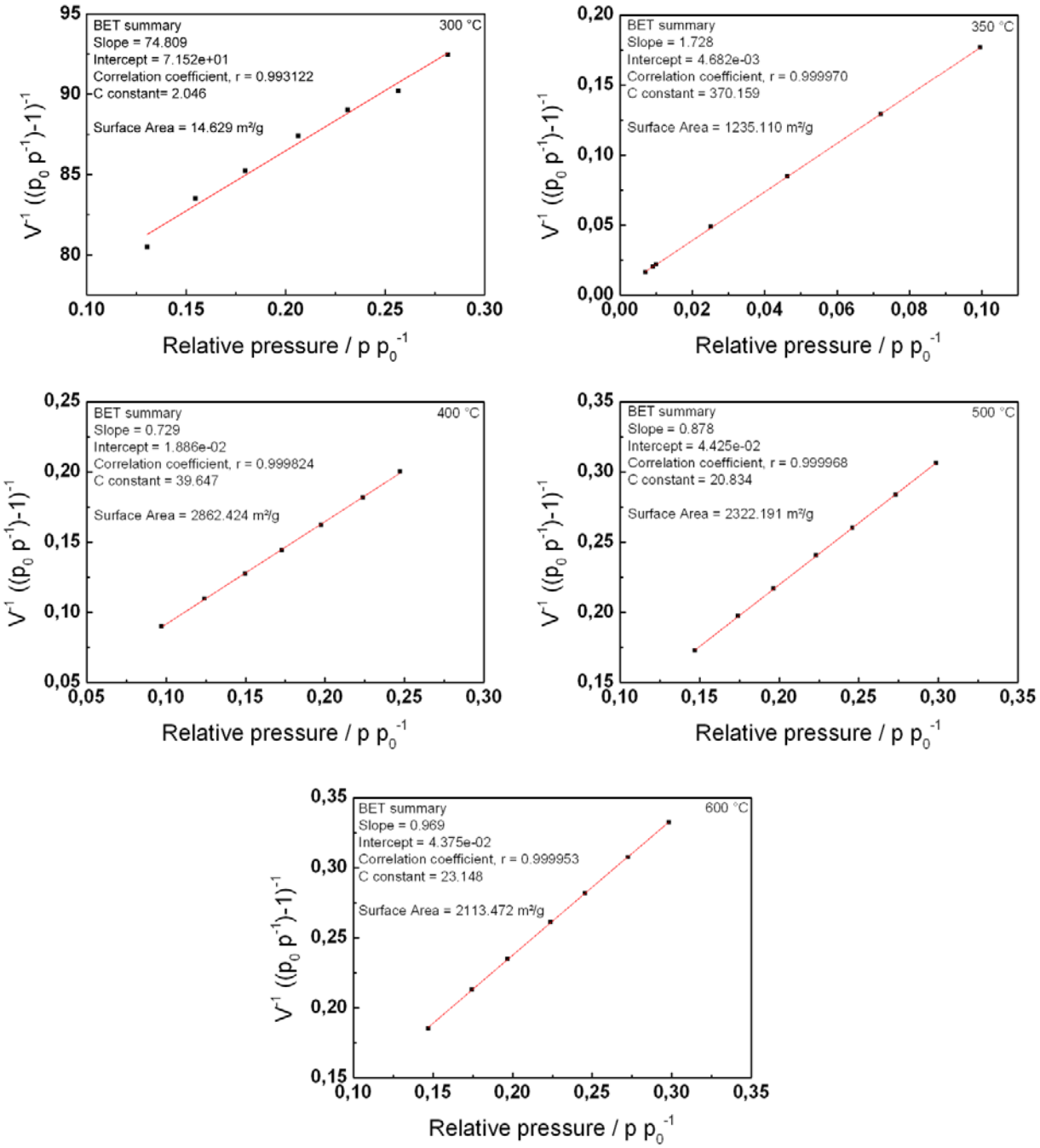

Figure S7. BET plots of the samples *fl*-CTF300, *fl*-CTF350, *fl*-CTF400, *fl*-CTF500 and *fl*-CTF600 from argon isotherms at 87 K.

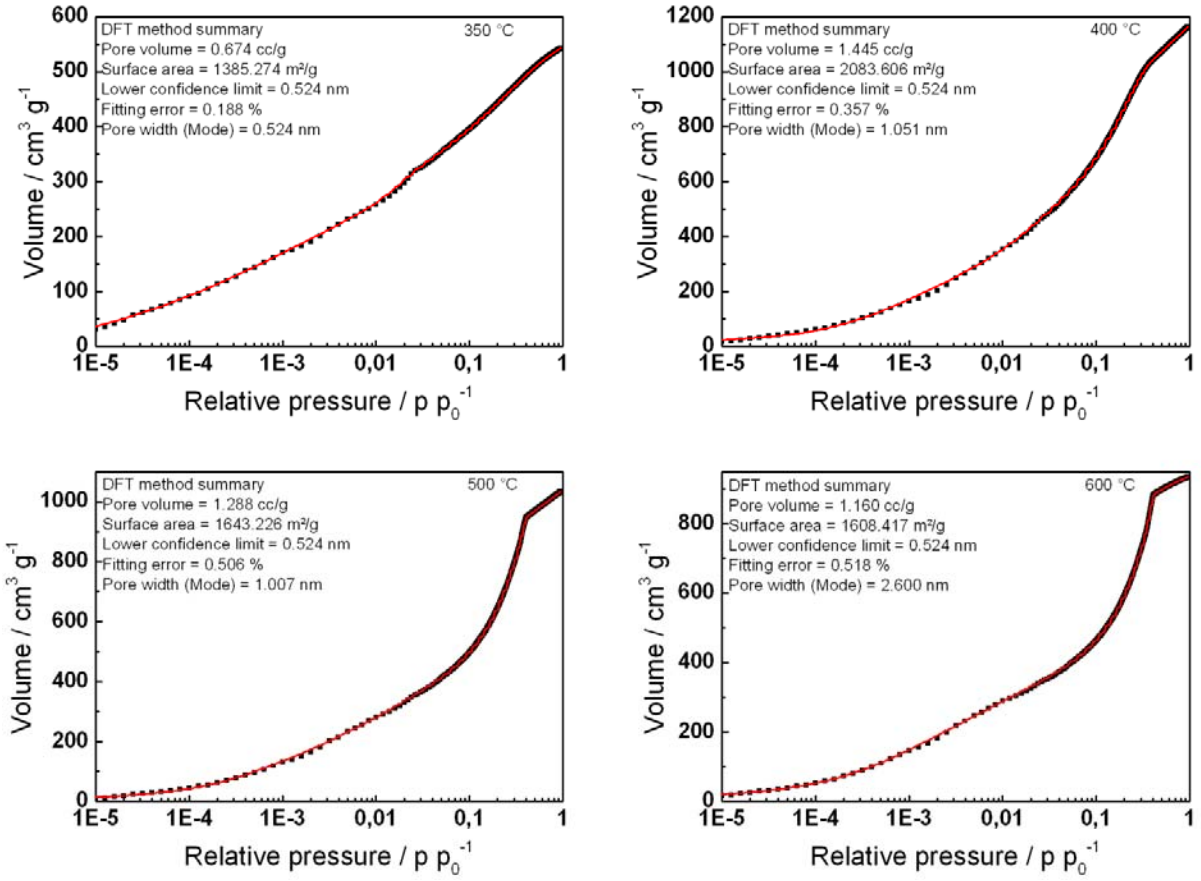

Figure S8. QSDFT fittings for the argon sorption isotherms of the samples *fl*-CTF350, *fl*-CTF400, *fl*-CTF500 and *fl*-CTF600.

6. H_2 Physisorption Measurements

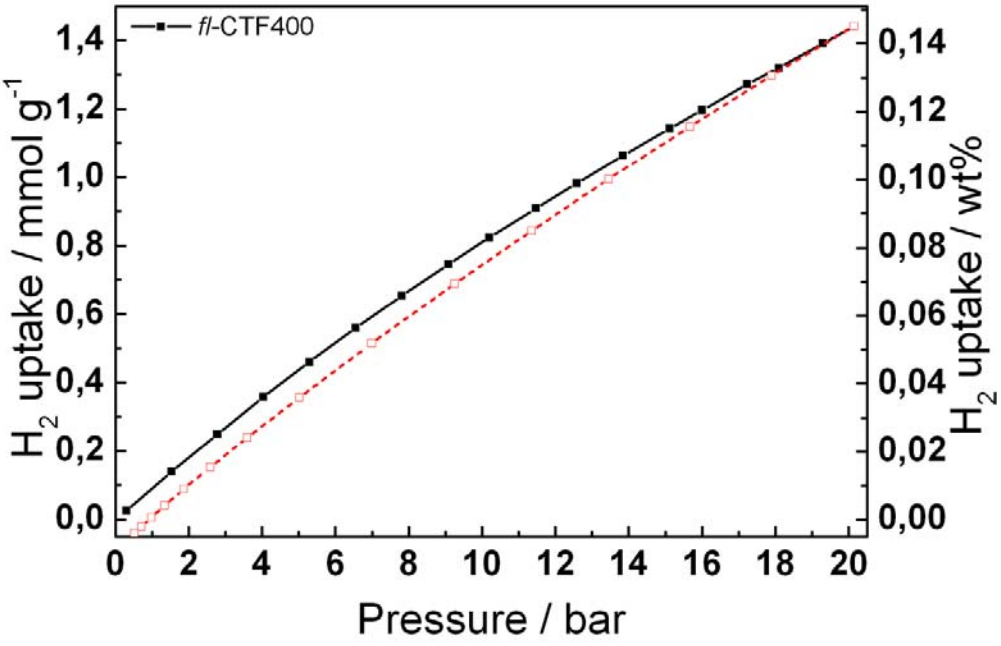

Figure S9. Hydrogen adsorption (filled symbols) and desorption (open symbols) isotherm of *fl*-CTF400 at 298 K.

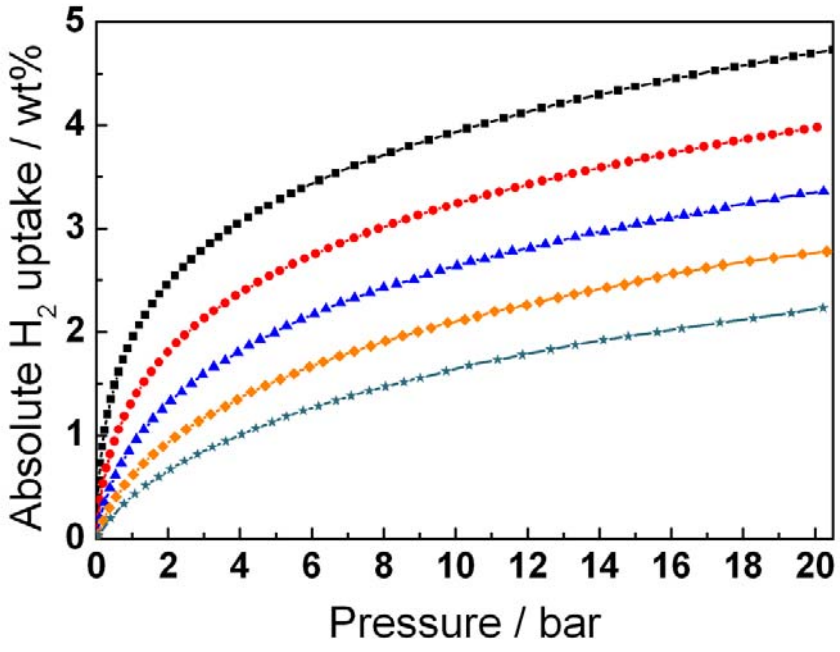

Figure S10. Fully reversible absolute hydrogen uptake in *fl*-CTF400 at 77, 87, 97, 107 and 117 K (from top to bottom).

c. Evaluation of the isosteric heat of adsorption

The isosteric heat of adsorption is calculated from the measured absolute isotherms according to the *Clausius-Clapeyron* equation

$$\Delta H = R \cdot \left(\frac{\partial \ln (P)}{\partial \frac{1}{T}} \right)_{\theta} \quad (2)$$

where θ is the surface coverage, R is the gas constant, P the pressure and T the temperature. Therefore ln(P) is plotted versus the reciprocal temperature 1/T for different surface coverages θ. The slope of the linear fit to this data for each surface coverage θ is proportional to the isosteric heat of adsorption.

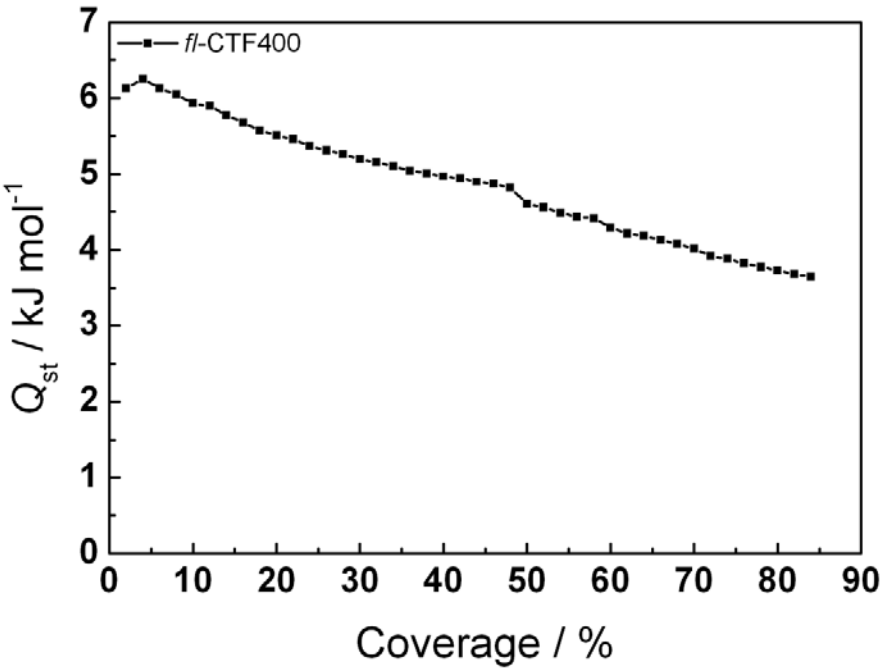

Figure S11. Heat of adsorption (Q_{st}) of *fl*-CTF400 calculated from the absolute hydrogen isotherms (77 K ~ 117 K) as a function of the normalized surface coverage.

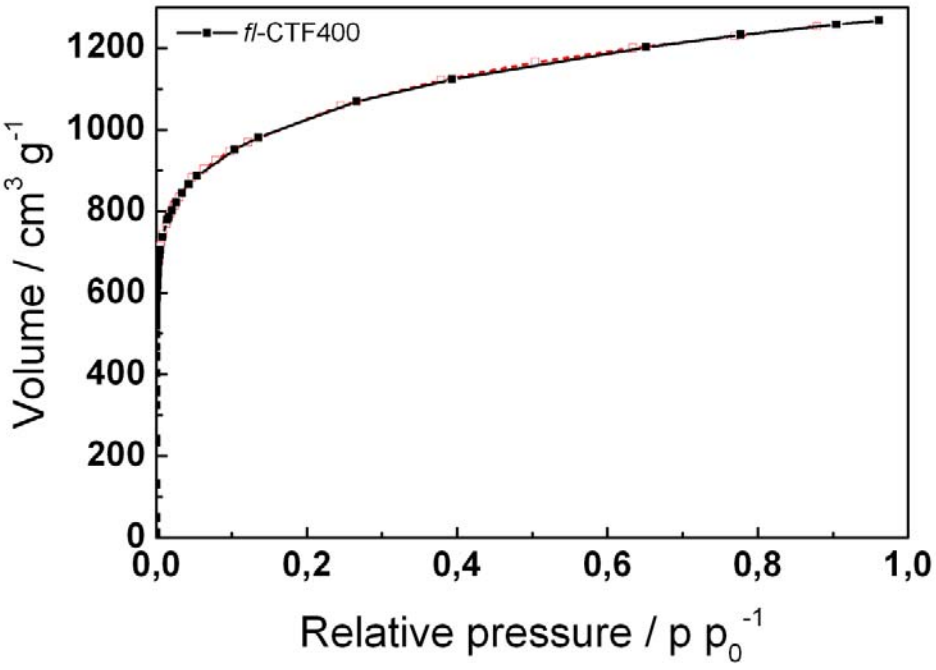

Figure S12. Low pressure hydrogen adsorption (filled symbols) and desorption (open symbols) isotherm of *fl*-CTF400 at 20 K.

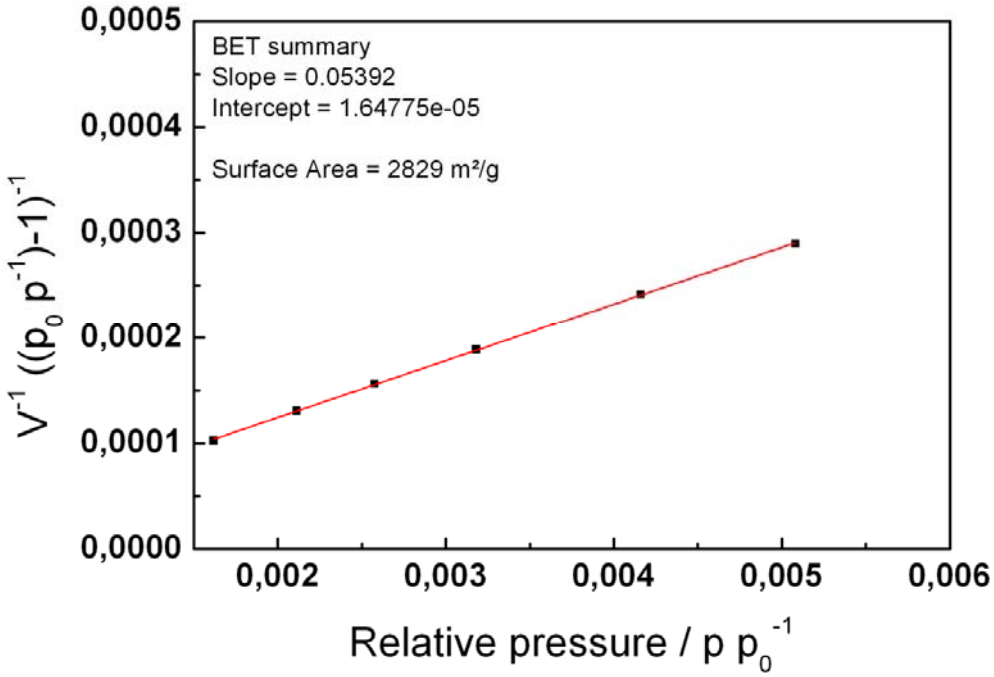

Figure S13. BET plot of *fl*-CTF400 from the hydrogen isotherm at 20 K.

Table S5. Textural characteristics of *fl*-CTF400 determined from hydrogen adsorption/desorption isotherms.

Sample	H_2 BET [$m^2\ g^{-1}$]	Pore Volume [a] [$cm^3\ g^{-1}$]	Excess H_2 uptake [wt%]			Skeletal density [$g\ cm^{-3}$]	Q_{st} [b] [$kJ\ mol^{-1}$]
			19.5 K, $p\ p_0^{-1} = 0.9$	77 K, p = 20 bar	298 K, p = 20 bar		
fl-CTF400	2829	1.6	10.2	4.4	0.15	1.6	4.9

[a]Total pore volume at $p\ p_0^{-1} = 0.9$, [b]Mean isosteric heat of hydrogen adsorption.

7. CO_2 Physisorption Measurements

Table S6. CO_2 and N_2 uptakes of *fl*-CTFs.

Sample	CO_2 uptake [$cm^3\ g^{-1}$][a] 273 K	298 K	313 K	N_2 uptake[b] [$cm^3\ g^{-1}$]
fl-CTF300	28.6	17.6	11.0	1.00
fl-CTF350	96.7	56.5	41.2	4.40
fl-CTF400	93.2	48.5	34.0	4.20
fl-CTF500	73.5	40.6	28.8	5.14
fl-CTF600	78.5	44.5	31.7	5.45

[a]At 1 bar. [b]At 1 bar and 298 K.

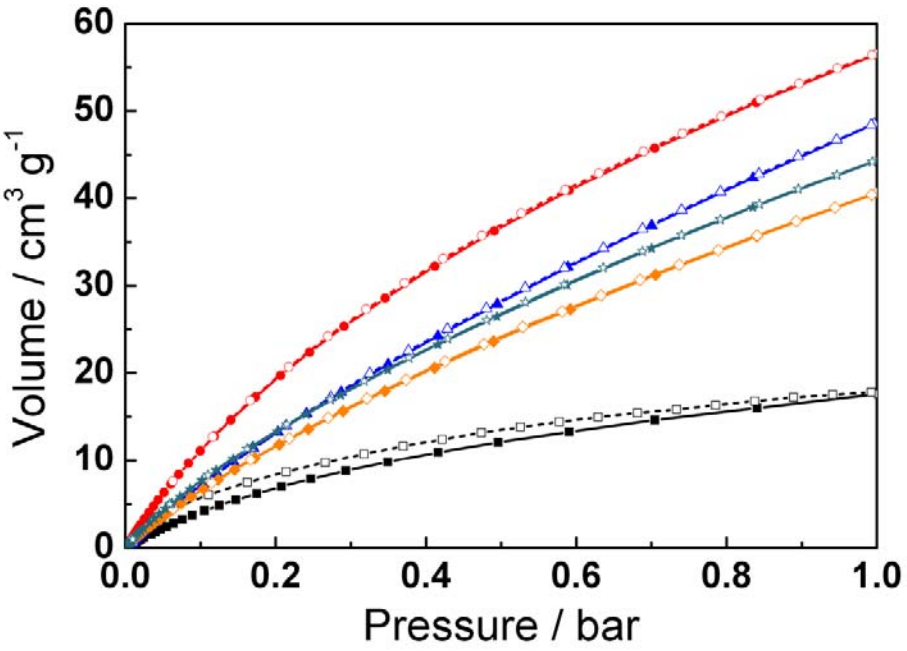

Figure S14. CO_2 adsorption (filled symbols) and desorption (open symbols) isotherms of the samples *fl*-CTF300, *fl*-CTF350, *fl*-CTF400, *fl*-CTF500 and *fl*-CTF600 at 298 K.

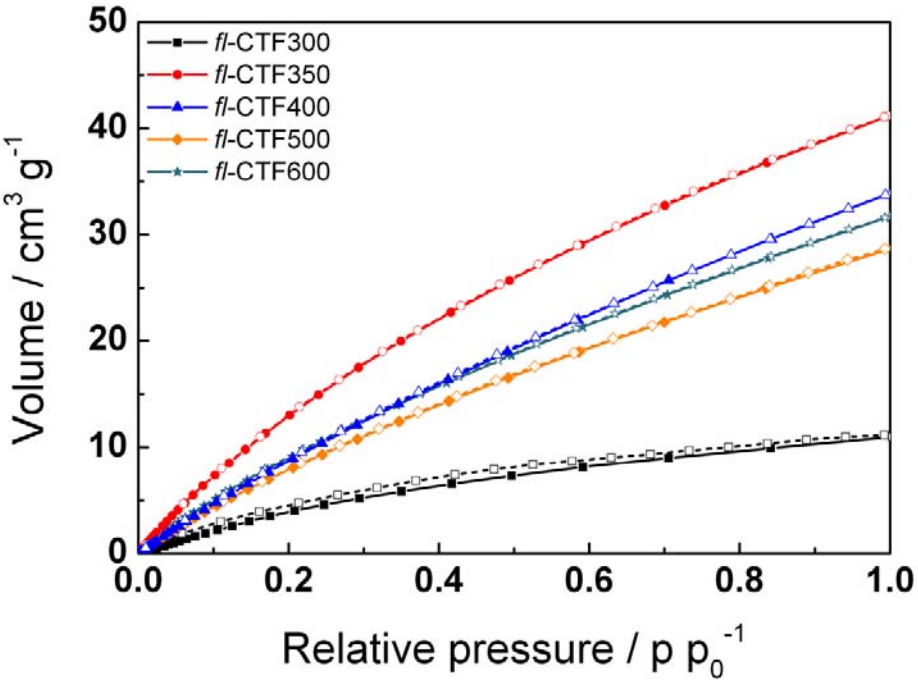

Figure S15. CO_2 adsorption (filled symbols) and desorption (open symbols) isotherms of the samples *fl*-CTF300, *fl*-CTF350, *fl*-CTF400, *fl*-CTF500 and *fl*-CTF600 at 313 K.

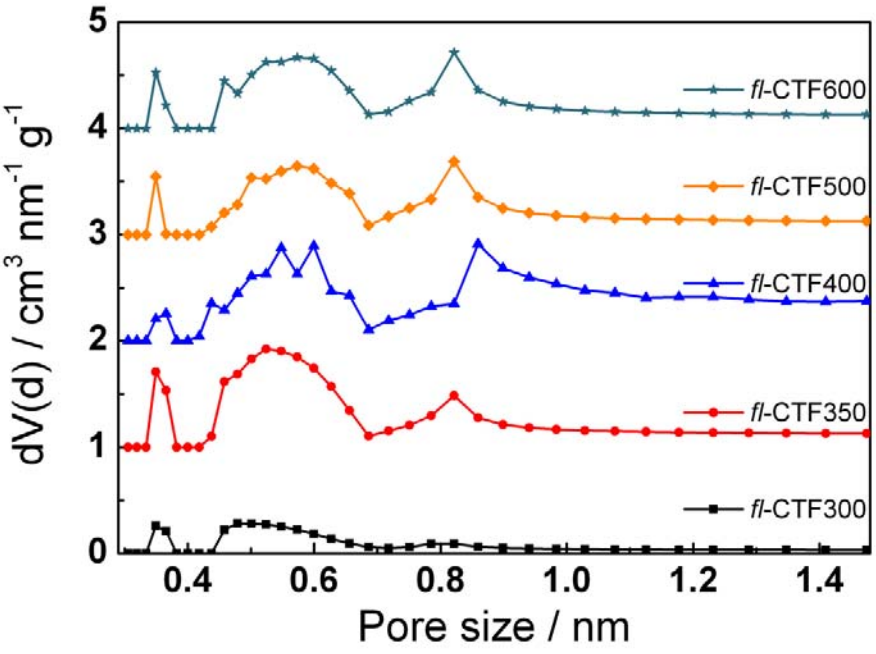

Figure S16. Pore size distributions of *fl*-CTF300, *fl*-CTF350, *fl*-CTF400, *fl*-CTF500 and *fl*-CTF600 from NLDFT calculations. The curves are shifted vertically in steps of 1 cm^3 nm^{-1} g^{-1}.

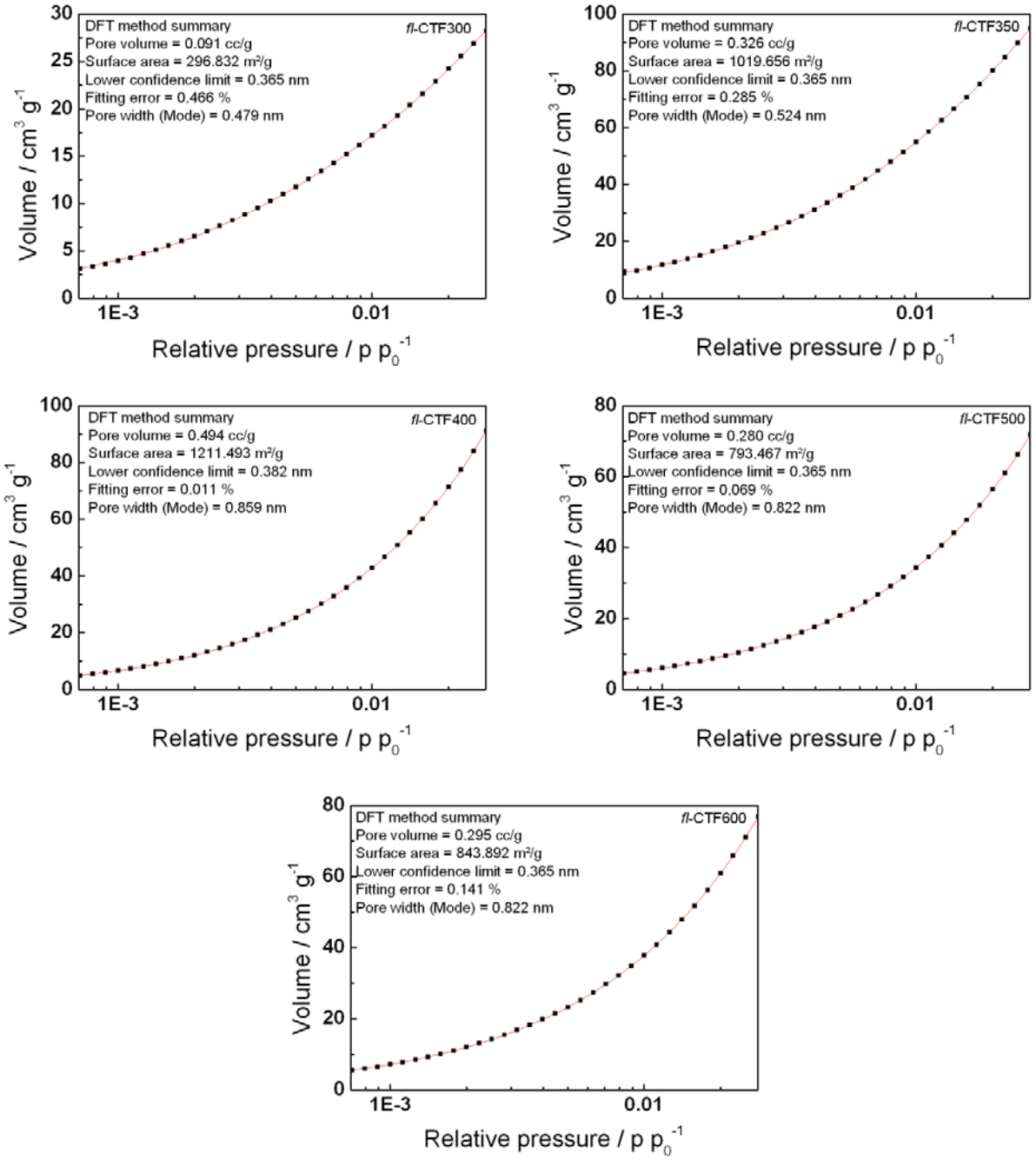

Figure S17. NLDFT-fittings for the argon isotherms of the samples *fl*-CTF300, *fl*-CTF350, *fl*-CTF400, *fl*-CTF500 and *fl*-CTF600.

8. N_2 Physisorption Measurements

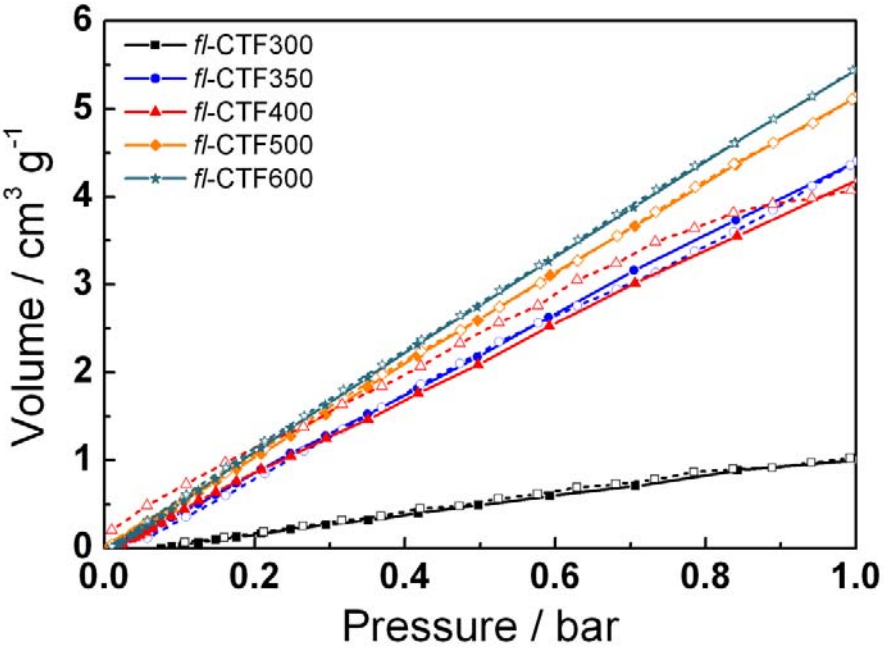

Figure S18. N_2 adsorption (filled symbols) and desorption (open symbols) isotherms of the samples *fl*-CTF300, *fl*-CTF350, *fl*-CTF400, *fl*-CTF500 and *fl*-CTF600 at 298 K.

9. CO_2/N_2 Selectivity Studies

a. Henry calculation

For selectivity calculations the ratio of the initial slopes in the *Henry* region of the adsorption isotherms of two different gases can be used.
The initial slopes are shown in Figure S18.

b. IAST calculation

Ideal adsorbed solution theory (IAST) calculations can be done by using a single or dual-site *Langmuir* model to fit the adsorption isotherms.[4]
The single-site *Langmuir* model is defined as,

$$q = \frac{q_{sat} b p}{1 + b p} \qquad (3)$$

q = molar loading of adsorbate
q_{sat} = saturation loading
b = *Langmuir* constant

The dual-site *Langmuir* model is defined as

$$q = q_A + q_B = \frac{q_{sat,A} b_A p}{1 + b_A p} + \frac{q_{sat,B} b_B p}{1 + b_B p} \quad (4)$$

A,B = distinct adsorption sites

For the fitting of the adsorption isotherms the single-site *Langmuir* model was used. The fitted graphs and the values of the parameters are shown in Figure S19.
The selectivities are calculated using following equation:

$$S = \frac{q_1/q_2}{p_1/p_2} \quad (5)$$

A CO_2:N_2 ratio of 15:85 was used for calculating the gas mixture selectivities.

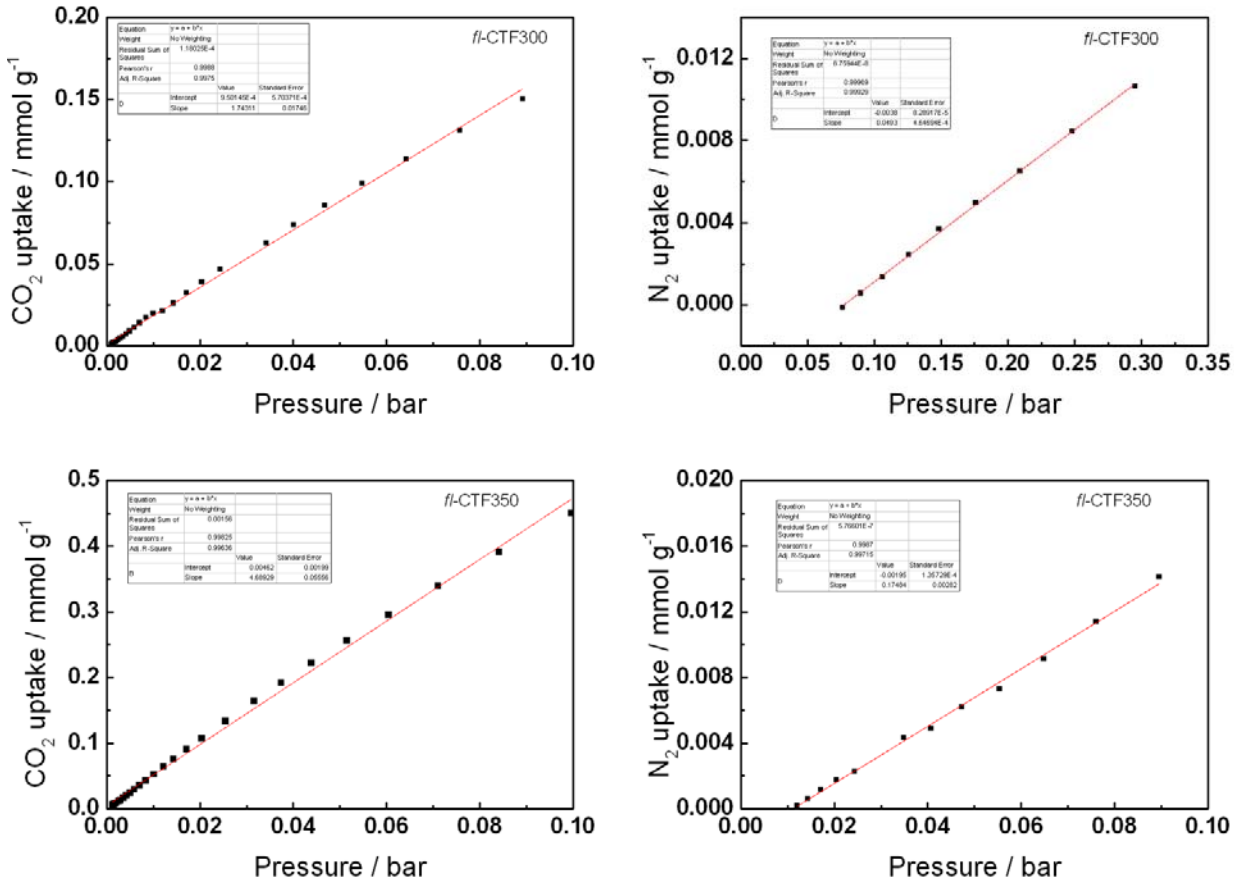

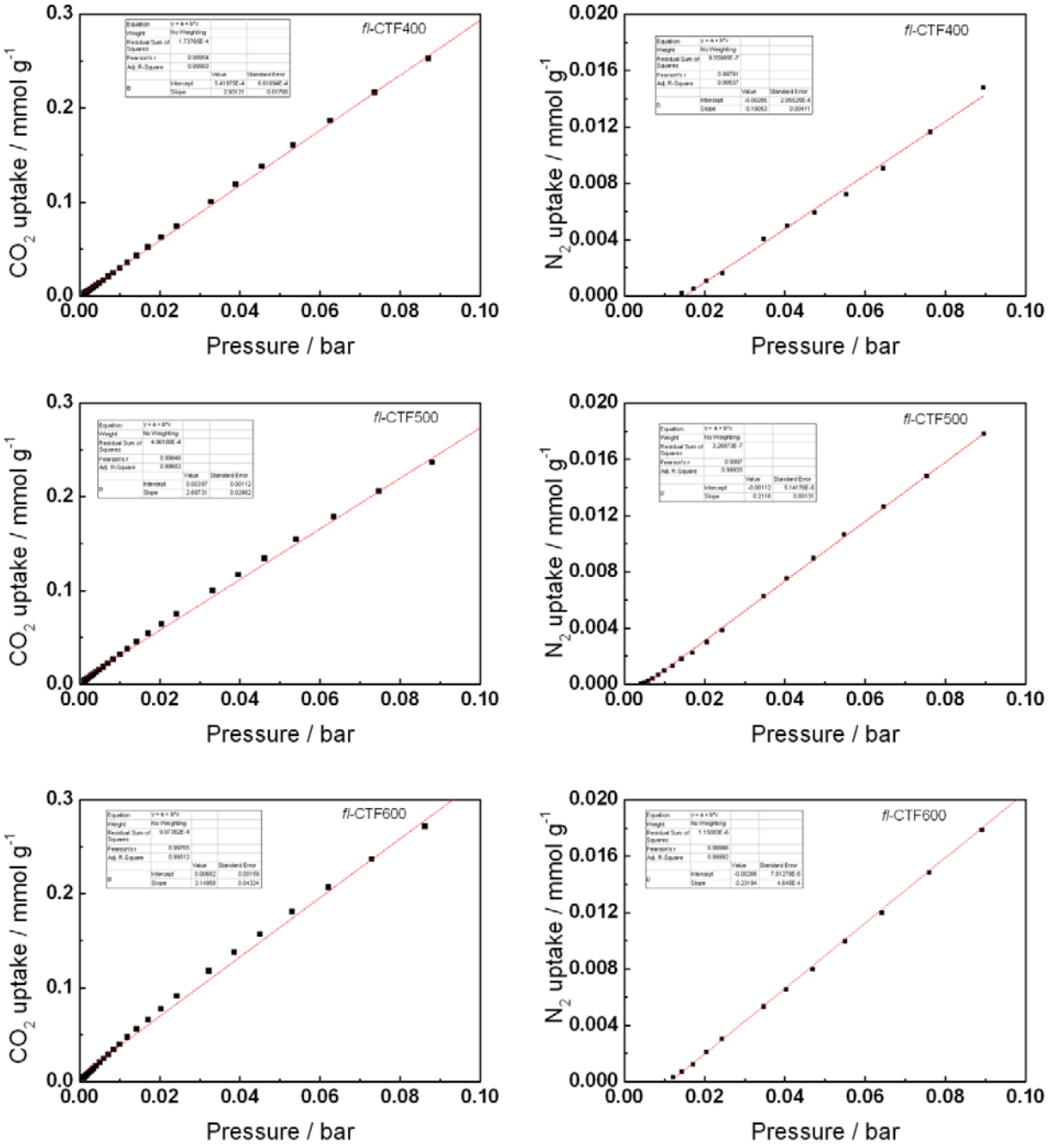

Figure S19. Henry plots of the samples *fl*-CTF300, *fl*-CTF350, *fl*-CTF400, *fl*-CTF500 and *fl*-CTF600 from CO_2 and N_2 isotherms at 298 K.

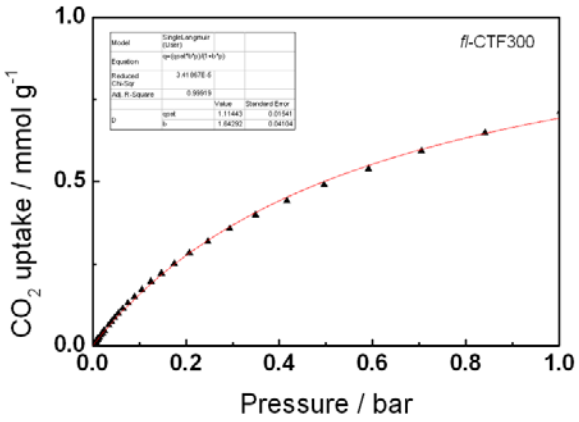
fl-CTF300
CO2 uptake / mmol g-1
Pressure / bar

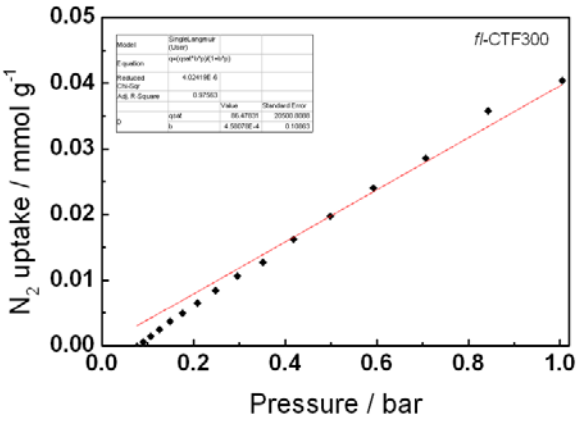
fl-CTF300
N2 uptake / mmol g-1
Pressure / bar

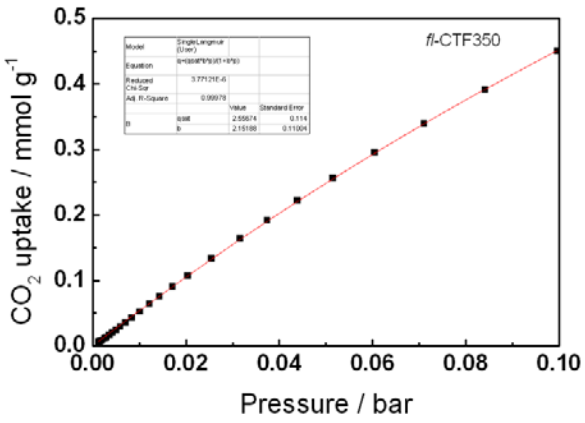
fl-CTF350
CO2 uptake / mmol g-1
Pressure / bar

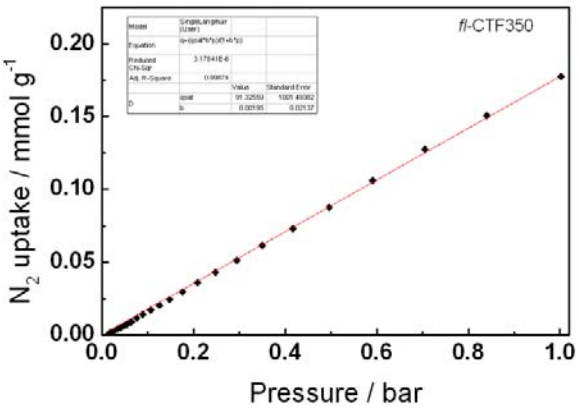
fl-CTF350
N2 uptake / mmol g-1
Pressure / bar

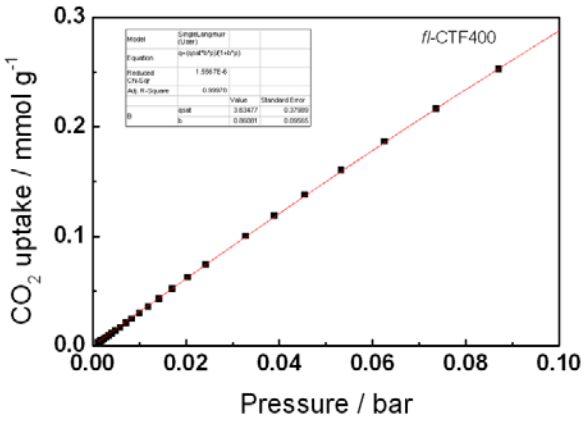
fl-CTF400
CO2 uptake / mmol g-1
Pressure / bar

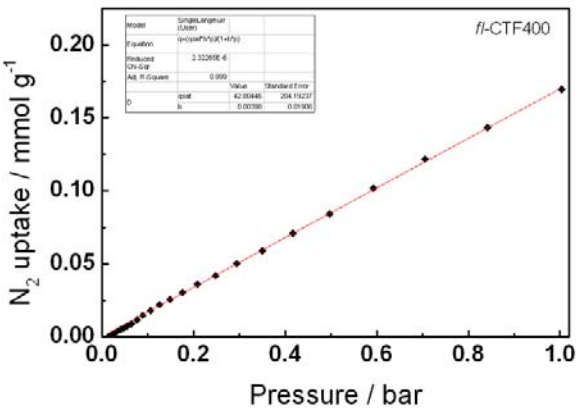
fl-CTF400
N2 uptake / mmol g-1
Pressure / bar

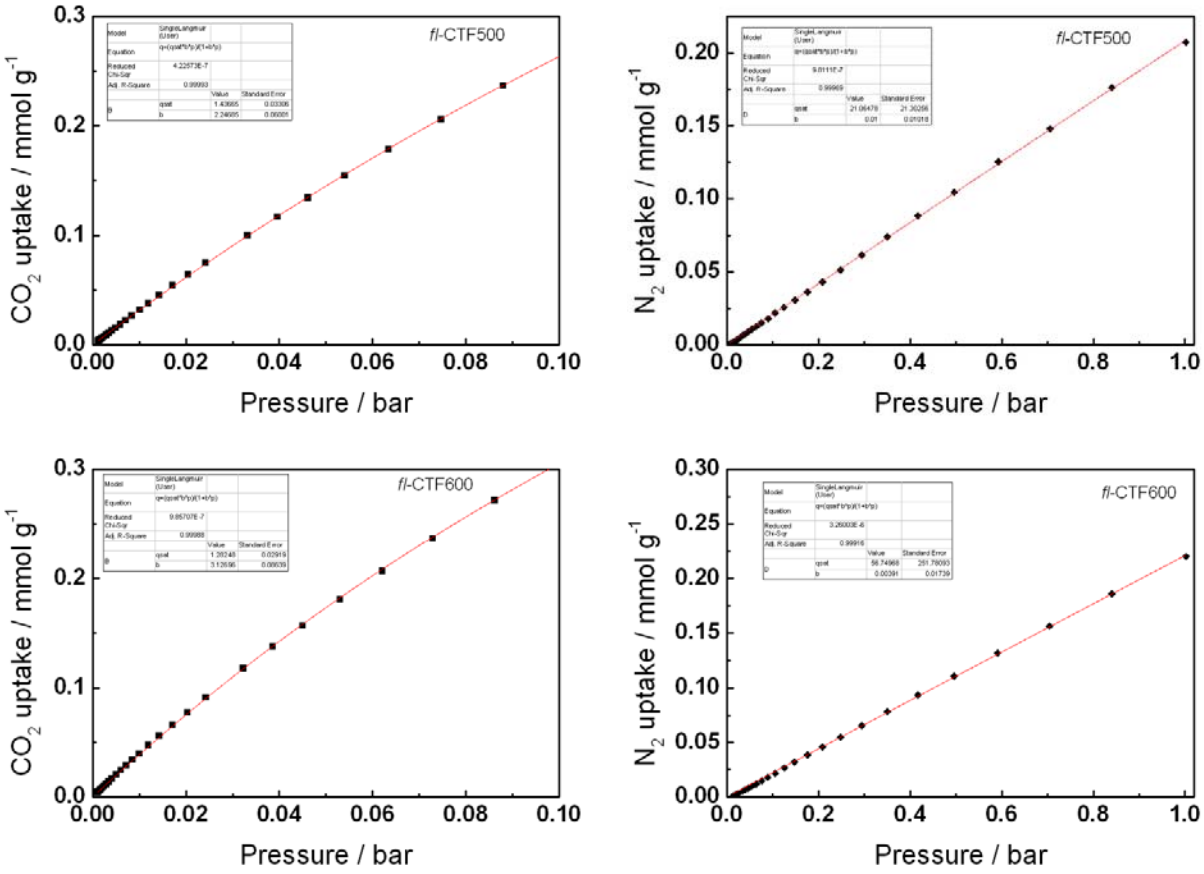

Figure S20. IAST-plots of the samples *fl*-CTF300, *fl*-CTF350, *fl*-CTF400, *fl*-CTF500 and *fl*-CTF600 from CO_2 and N_2 isotherms at 298 K.

10.Liquid NMR spectra

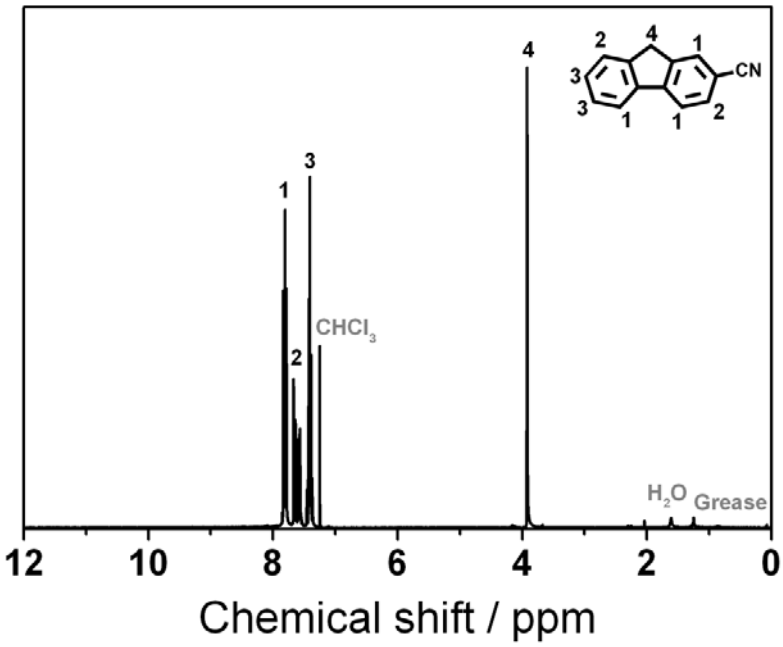

Figure S21. ^{1}H NMR spectrum of 9*H*-fluorene-2-carbonitrile.

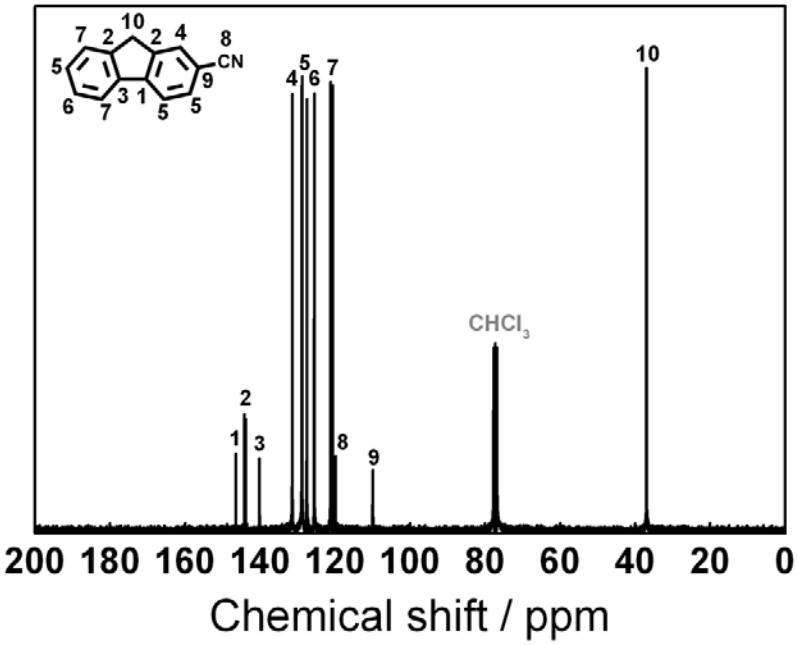

Figure S22. ^{13}C NMR spectrum of 9*H*-fluorene-2-carbonitrile.

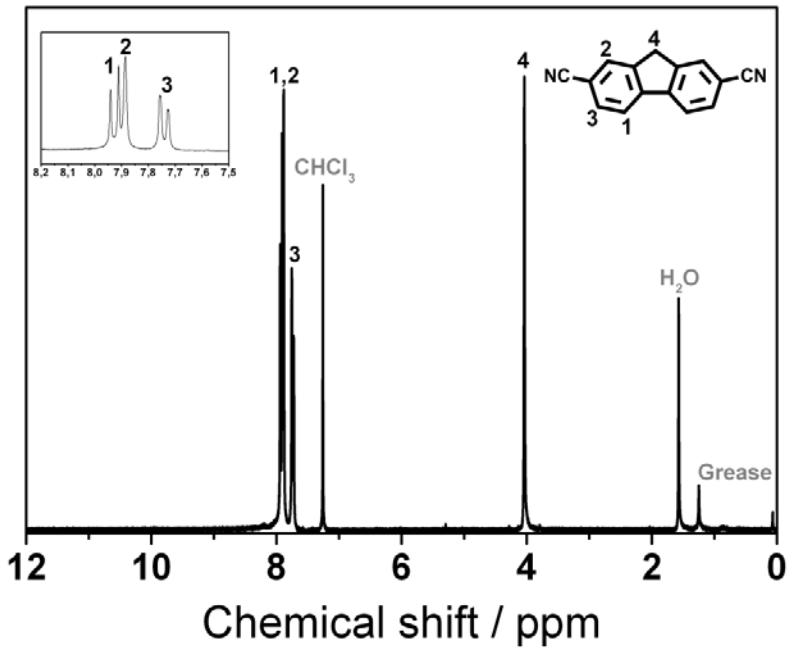

Figure S23. ^{1}H NMR spectrum of 9*H*-fluorene-2,7-dicarbonitrile.

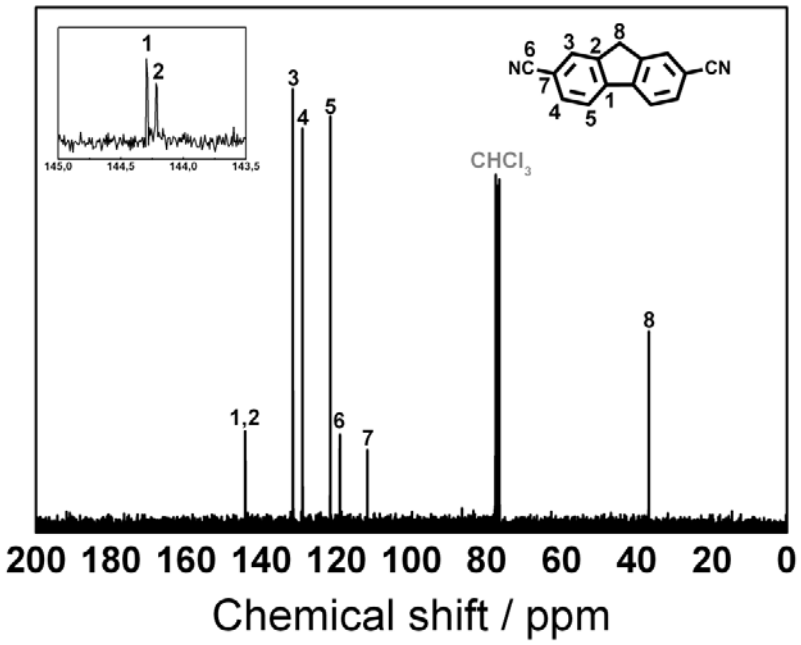

Figure S24. ^{13}C NMR spectrum of 9*H*-fluorene-2,7-dicarbonitrile.

11. DTA/TG measurements

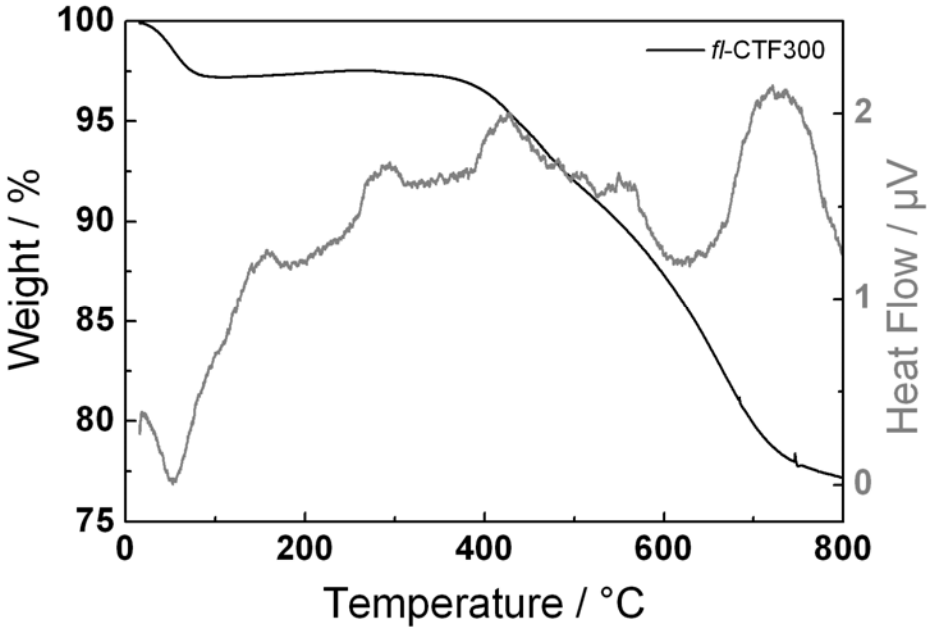

Figure S25. DTA/TG measurement of *fl*-CTF300.

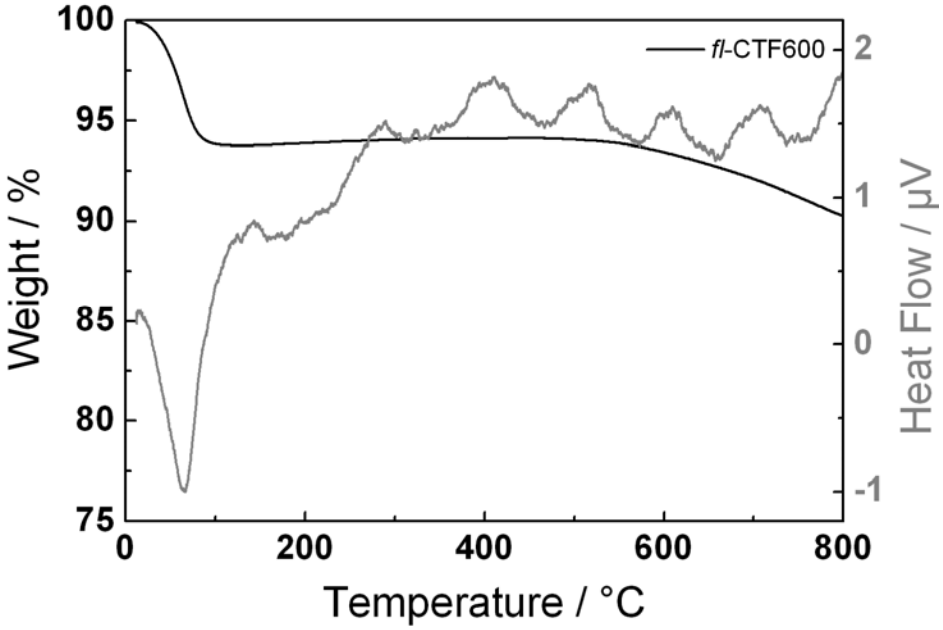

Figure S26. DTA/TG measurement of *fl*-CTF600.

12.Comparison of the CO_2 adsorption characteristics of POPs

Table S7. Comparison of the CO_2 capacities, selectivities and heats of adsorption of some reported POPs.

POP	Porosity [$m^2\ g^{-1}$]	CO_2 capacity [mmol g^{-1}]		Q_{st} [kJ mol^{-1}]	Selectivity over N_2[b]		References
	BET	273 K	298 K		Henry	IAST	
APOP-1	1298	4.26	2.69	26.6	20.3		[5]
APOP-1-OH	875	2.89	1.86	30.0	26.0		
APOP-1-ONa	760	2.89	1.71	30.6	29.2		
APOP-1-F	724	3.07	2.02	33.3	31.8		
APOP-2	906	2.27	1.30	31.7	20.2		
APOP-3	1402	4.45	2.59	27.5	26.0		
APOP-4	833	2.70	1.64	30.7	23.3		
azo-COP-1	635	2.44	1.48	29.3	113	97	[6]
azo-COP-2	729	2.55	1.53	24.8	142	131	
azo-COP-3	493	1.93	1.22	32.1	122	96	
BILP-1	1172	4.27	2.98	26.5	36		[7]
BILP-2	708	3.89	2.36	28.6	71		[8]
BILP-3	1306	5.11	3.30	28.6	31		
BILP-4	1135	5.34	3.59	28.7	32		
BILP-5	599	2.91	1.98	28.8	36		
BILP-6	1261	4.80	2.75	28.4	39		
BILP-7	1122	4.39	2.77	27.8	34		
BILP-10	787	4.02	~2.5	38.2	59	107	[9]
BLP-1	1360	1.82	0.97	25.3			[10]
BLP-12	2244	3.34	1.82	25.2			
CMP-1	837	2.05	1.18	~27			[11]
COF-1	750	2.32					[12,13]
COF-5	1670	1.34					
COF-6	750	3.84					
COF-8	1350	1.43					
COF-10	1760	1.21					
COF-102	3620	1.56					
COF-103	3530	1.70					
COP-3	413	1.68	1.14	24.5	24	107	[14]

CTF-0	2011	4.22				[15]
CTF-1	746	2.47	1.41	~27.5	20	[16]
CTF-1-600	1553	3.82	2.25	~30.0	13	
CTF-P2	776	1.88			20[c]	[17]
CTF-P3	571	2.27			23[c]	
CTF-P4	867	3.12			17[c]	
CTF-P5	960	3.00			24[c]	
CTF-P6	1152	3.39			16[c]	
CTF-P1M	4	0.94			31[c]	
CTF-P2M	464	1.91			21[c]	
CTF-P3M	523	2.26			16[c]	
CTF-P4M	542	1.87			22[c]	
CTF-P5M	542	2.08			20[c]	
CTF-P6M	947	4.20			14[c]	
FCTF-1	662	4.67	3.21	35.0	31	[16]
FCTF-1-600	1535	5.53	3.41	~32	19	
HCP 1	1646	3.01	1.7	23.5		[18]
HCP 2	1684	3.30	1.7	21.2		
HCP 3	1531	3.24	1.6	22.1		
HCP 4	1642	3.92	1.6	21.6		
HCP-BDM	847	2.87	~1.7	33.5	27	[19]
HCP-BA	742	1.92	~1.1	27.4	19	
HCP-BC	746	1.91	~1.1			
HMP Th-1	726	2.88	~1.7	27	39[c]	[20]
HMP Py-1	437	2.71	~1.7	36	117[c]	
HMP Fu-1	514	2.21	~1.4	28	50[c]	
ILCOF-1	2723	1.36	~0.8	18.3		[21]
ILP	744	1.97	1.05			[22]
NC-600	366	2.33	1.65	~49		
NC-700	284	2.13	1.80	~49		
NC-800	263	2.65	1.95	~45		
MCTF300	640	2.25	1.41	24.6		[23]
MCTF400	1060	2.37	1.60	25.4		
MCTF500	1510	3.16	2.26	26.3		

MOP-A (PAF-1)	4077	2.65	1.45	~24	9	8	[12]
MOP-B (COF-300)	1847	3.29	1.63	~22	20	21	
MOP-C (Click network)	1237	3.86	2.20	33	14	20	
MOP-D (Tetrahedral-CMP)	1213	2.42	1.3	~26	12	15	
MOP-E (TPM-HCP)	140	2.95	1.77	~25	9	12	
MOP-F (CMP-NH2CH3)	653	1.80	1.08	~27	12	18	
MOP-G (CMP carbazole)	1056	2.15	1.25	~27	15	25	
MOP A-B1	378	2.67	2.01[a]	30.0		68[c]	[24]
MOP A-B2	614	2.71	1.90[a]	33.4		56[c]	
MOP A-B3	589	2.24	1.71[a]	28.4		65[c]	
MPI-1	1454	3.81	~2.2	34.8	102[c]		[25]
MPI-2	814	3.14	~2.2	30.4	71[c]		
MPI-3	586	2.25	~1.7	31.4	41[c]		
NPAF	1790	3.64	2.32	19		88	[26]
NPOF-4	1249	2.50	1.40	23.2	16	12	[27]
NPOF-4-NO_2	337	2.42	1.56	32.5	66	59	
NPOF-4-NH_2	554	2.90	1.88	30.1	40	38	
PAF-1	5460	2.07	1.09	15.6	38[c]		[28]
PAF-3	2932	3.51	1.84	19.2	87[c]		
PAF-4	2246	2.43	1.16	16.2	44[c]		
PAF-1-350	4033	3.10		21.2			[29]
PAF-1-380	2881	3.37		23.6			
PAF-1-400	2292	3.71		26.7			
PAF-1-450	1191	4.50		27.8		209[c]	
PAF-16-2	979	1.90	1.18	30.3			[30]
PBI-1	62	3.00	~1.6	34.2			[31]
PBI-2	85	1.02	~0.2	32.4			
PCTF-1	2235	3.23	1.89[a]	30	13[c]	14[c]	[32,33]
PCTF-2	784	1.84	1.02[a]	26	9[c]	14[c]	

PCTF-3	641	2.16	1.36[a]	27	16[c]	25[c]	32
PCTF-4	1090	2.29	1.53[a]	28	17[c]	26[c]	
PCTF-5	1183	2.57	1.52[a]	27	17[c]	32[c]	
PCTF-7	613	2.17	1.35[a]	25	22[c]	41[c]	
PECONF-1	499	1.86	1.34	29	51		34
PECONF-2	637	2.85	1.98	31	44		
PECONF-3	851	3.49	2.47	26	41		
PECONF-4	-	2.95	1.96	34	51		
PI-1	506	~2.0	1.41	34	27		35
PI-2	568	~1.5	1.00	27	12		
PI1	660	1.66					36
PI2	265	0.61					
PI3	366	1.36					
PIF	39		0.31				37
PIF-5	121		1.35				
PIF-6	527		3.20	42.7	59		
PIF-7	1038		3.42				
PIF-8	1185		2.75				
POF1B	917	4.23	2.16				38
PP-N-100	318	2.54		~40			39
PP-N-75	689	3.13		~37			
PP-N-50	1141	3.86		~35			
PP-N-25	1257	4.60		~34			
PP-N-0	1530	3.90		~26			
PPF-1	1740	6.12		25.6		15[c]	40
PPF-2	1470	5.54		29.2		15[c]	
PPF-3	419	2.09		21.8		20[c]	
PPF-4	726	2.59		25.1		15[c]	
PPN-6-CH_2DETA	555		4.30	~56		442[e]	41
SMPI-0	574	2.53	1.43	36	30[c]		42
SMPI-10	112	3.15	1.87	33	32[c]		
SMPI-50	44	2.96	1.61	30	48[c]		
SMPI-100	23	2.82	1.87	30	58[c]		
SNU-C1-va	595	3.49	2.31	34.9			43
SNU-C1-sca	830	4.38	3.14	31.2			
STP-1	1305	3.67					44
STP-2	1990	4.14					

TB-MOP	694	4.05	2.57	29.5	51	[45]
TC-EMC	3840		3.3	30	1.3	[46]
TC-Y1	3519		3.0			
TC-Y2	1815		1.6			
N-TC-EMC	2559		4.0	50	6.1	
N-TC-Y1	1762		3.2			
N-TC-Y2	1361		2.6			
TDCOF-5	2497	2.1	~1.2	21.8		[47]
TPI-1	809	2.45	1.25	34.4	31	[48]
TPI-2	796	2.45	1.23	31.4	34	
TPI-3	40	0.68	0.43	32.3	35	
TPI-4	245	1.85	1.11	33.6	46	
TPI-5	201	1.57	0.96	30.0	46	
TPI-6	510	2.02	1.10	29.2	34	
TPI-7	<10	1.81	1.10	32.4	56	
TpPa-1	535	3.54				[49]
TpPa-NO_2	129	3.23				
TpPa-2	339	2.79				
TpBD-$(NO_2)_2$	295	2.30				
TpBD	537	1.78				
TpBD-Me_2	468	1.64				
TpPa-F_4	438	1.55				
TpBD-$(OMe)_2$	330	1.20				
O-TTPP	593	2.26	1.56	28.6	21	[50]
S-TTPP	606	1.81	1.04	28.0	22	

[a] at 293K, [b] at 298 K, [c] at 273K, [d] "break through" measurement adjustment, [e] at 295K.

1. X. L. Wu and K. W. Zilm, *J. Magn. Reson. A*, 1993, **102**, 205-213.
2. B. Jürgens, E. Irran, J. Senker, P. Kroll, H. Müller and W. Schnick, *J. Am. Chem. Soc.*, 2003, **125**, 10288-10300.
3. C. Gervais, F. Babonneau, J. Maquet, C. Bonhomme, D. Massiot, E. Framery and M. Vaultier, *Magn. Reson. Chem.*, 1998, **36**, 407-414.
4. A. L. Myers and J. M. Prausnitz, *AIChE J.*, 1965, **11**, 121-127.
5. W.-C. Song, X.-K. Xu, Q. Chen, Z.-Z. Zhuang and X.-H. Bu, *Polym. Chem.*, 2013, **4**, 4690-4696.
6. H. A. Patel, S. Hyun Je, J. Park, D. P. Chen, Y. Jung, C. T. Yavuz and A. Coskun, *Nat Commun*, 2013, **4**, 1357.
7. M. G. Rabbani and H. M. El-Kaderi, *Chem. Mater.*, 2011, **23**, 1650-1653.
8. M. G. Rabbani and H. M. El-Kaderi, *Chem. Mater.*, 2012, **24**, 1511-1517.

9. M. G. Rabbani, A. K. Sekizkardes, O. M. El-Kadri, B. R. Kaafarani and H. M. El-Kaderi, *J. Mater. Chem.*, 2012, **22**, 25409-25417.
10. K. T. Jackson, M. G. Rabbani, T. E. Reich and H. M. El-Kaderi, *Polym. Chem.*, 2011, **2**, 2775-2777.
11. R. Dawson, D. J. Adams and A. I. Cooper, *Chemical Science*, 2011, **2**, 1173-1177.
12. R. Dawson, E. Stockel, J. R. Holst, D. J. Adams and A. I. Cooper, *Energy Environ. Sci.*, 2011, **4**, 4239-4245.
13. H. Furukawa and O. M. Yaghi, *J. Am. Chem. Soc.*, 2009, **131**, 8875-8883.
14. H. A. Patel, F. Karadas, J. Byun, J. Park, E. Deniz, A. Canlier, Y. Jung, M. Atilhan and C. T. Yavuz, *Adv. Funct. Mater.*, 2013, **23**, 2270-2276.
15. P. Katekomol, J. Roeser, M. Bojdys, J. Weber and A. Thomas, *Chem. Mater.*, 2013, **25**, 1542-1548.
16. Y. Zhao, K. X. Yao, B. Teng, T. Zhang and Y. Han, *Energy Environ. Sci.*, 2013, **6**, 3684-3692.
17. S. Ren, M. J. Bojdys, R. Dawson, A. Laybourn, Y. Z. Khimyak, D. J. Adams and A. I. Cooper, *Adv. Mater. (Weinheim, Ger.)*, 2012, **24**, 2357-2361.
18. C. F. Martin, E. Stockel, R. Clowes, D. J. Adams, A. I. Cooper, J. J. Pis, F. Rubiera and C. Pevida, *J. Mater. Chem.*, 2011, **21**, 5475-5483.
19. Y. Luo, S. Zhang, Y. Ma, W. Wang and B. Tan, *Polym. Chem.*, 2013, **4**, 1126-1131.
20. Y. Luo, B. Li, W. Wang, K. Wu and B. Tan, *Adv. Mater. (Weinheim, Ger.)*, 2012, **24**, 5703-5707.
21. M. G. Rabbani, A. K. Sekizkardes, Z. Kahveci, T. E. Reich, R. Ding and H. M. El-Kaderi, *Chem. Eur. J.*, 2013, **19**, 3324-3328.
22. J. Wang, I. Senkovska, M. Oschatz, M. R. Lohe, L. Borchardt, A. Heerwig, Q. Liu and S. Kaskel, *ACS Appl. Mater. Interfaces*, 2013, **5**, 3160-3167.
23. X. Liu, H. Li, Y. Zhang, B. Xu, S. A, H. Xia and Y. Mu, *Polym. Chem.*, 2013, **4**, 2445-2448.
24. C. Xu and N. Hedin, *J. Mater. Chem. A*, 2013, **1**, 3406-3414.
25. G. Li and Z. Wang, *Macromolecules*, 2013, **46**, 3058-3066.
26. D. E. Demirocak, M. K. Ram, S. S. Srinivasan, D. Y. Goswami and E. K. Stefanakos, *J. Mater. Chem. A*, 2013, **1**, 13800-13806.
27. T. Islamoglu, M. Gulam Rabbani and H. M. El-Kaderi, *J. Mater. Chem. A*, 2013, **1**, 10259-10266.
28. T. Ben, C. Pei, D. Zhang, J. Xu, F. Deng, X. Jing and S. Qiu, *Energy Environ. Sci.*, 2011, **4**, 3991-3999.
29. T. Ben, Y. Li, L. Zhu, D. Zhang, D. Cao, Z. Xiang, X. Yao and S. Qiu, *Energy Environ. Sci.*, 2012, **5**, 8370-8376.
30. W. Wang, H. Ren, F. Sun, K. Cai, H. Ma, J. Du, H. Zhao and G. Zhu, *Dalton Trans.*, 2012, **41**, 3933-3936.
31. H. Yu, M. Tian, C. Shen and Z. Wang, *Polym. Chem.*, 2013, **4**, 961-968.
32. A. Bhunia, I. Boldog, A. Moller and C. Janiak, *J. Mater. Chem. A*, 2013, **1**, 14990-14999.
33. A. Bhunia, V. Vasylyeva and C. Janiak, *Chem. Commun. (Cambridge, U. K.)*, 2013, **49**, 3961-3963.
34. P. Mohanty, L. D. Kull and K. Landskron, *Nat Commun*, 2011, **2**, 401.
35. A. Laybourn, R. Dawson, R. Clowes, J. A. Iggo, A. I. Cooper, Y. Z. Khimyak and D. J. Adams, *Polym. Chem.*, 2012, **3**, 533-537.
36. Y. Luo, B. Li, L. Liang and B. Tan, *Chem. Commun. (Cambridge, U. K.)*, 2011, **47**, 7704-7706.
37. M. Saleh, J. N. Tiwari, K. C. Kemp, M. Yousuf and K. S. Kim, *Environ. Sci. Technol.*, 2013.
38. A. P. Katsoulidis and M. G. Kanatzidis, *Chem. Mater.*, 2011, **23**, 1818-1824.
39. Y. Yang, Q. Zhang, S. Zhang and S. Li, *Polymer*, 2013, **54**, 5698-5702.
40. Y. Zhu, H. Long and W. Zhang, *Chem. Mater.*, 2013, **25**, 1630-1635.

41. W. Lu, J. P. Sculley, D. Yuan, R. Krishna, Z. Wei and H.-C. Zhou, *Angew. Chem. Int. Ed.*, 2012, **51**, 7480-7484.
42. Y. Yang, Q. Zhang, Z. Zhang and S. Zhang, *J. Mater. Chem. A*, 2013, **1**, 10368-10374.
43. L.-H. Xie and M. P. Suh, *Chem. Eur. J.*, 2013, **19**, 11590-11597.
44. C. Zhang, Y. Liu, B. Li, B. Tan, C.-F. Chen, H.-B. Xu and X.-L. Yang, *ACS Macro Lett.*, 2011, **1**, 190-193.
45. X. Zhu, C.-L. Do-Thanh, C. R. Murdock, K. M. Nelson, C. Tian, S. Brown, S. M. Mahurin, D. M. Jenkins, J. Hu, B. Zhao, H. Liu and S. Dai, *ACS Macro Lett.*, 2013, **2**, 660-663.
46. L. Wang and R. T. Yang, *J. Phys. Chem. C*, 2011, **116**, 1099-1106.
47. Z. Kahveci, T. Islamoglu, G. A. Shar, R. Ding and H. M. El-Kaderi, *CrystEngComm*, 2013, **15**, 1524-1527.
48. M. R. Liebl and J. Senker, *Chem. Mater.*, 2013, **25**, 970-980.
49. S. Chandra, S. Kandambeth, B. P. Biswal, B. Lukose, S. M. Kunjir, M. Chaudhary, R. Babarao, T. Heine and R. Banerjee, *J. Am. Chem. Soc.*, 2013, **135**, 17853-17861.
50. X. Chen, S. Qiao, Z. Du, Y. Zhou and R. Yang, *Macromol. Rapid Commun.*, 2013, **34**, 1181-1185.